**The Cryosphere
Discussions**

A new bed elevation dataset for Greenland

J. A. Griggs[1], **J. L. Bamber**[1], **R. T. W. L., Hurkmans**[1], **J. A. Dowdeswell**[2],
S. P. Gogineni[3], **I. Howat**[4,5], **J. Mouginot**[6], **J. Paden**[3], **S. Palmer**[2], **E. Rignot**[6,7],
and D. Steinhage[8]

[1]Bristol Glaciology Centre, School of Geographical Sciences, University of Bristol, Bristol, UK
[2]University of Cambridge, Scott Polar Research Institute, Cambridge UK
[3]University of Kansas, Center for Remote Sensing Ice Sheets, Lawrence, Kansas, USA
[4]Ohio State University, School of Earth Sciences, Columbus, Ohio, USA
[5]Ohio State University, Byrd Polar Research Center, Columbus, Ohio USA
[6]University of California Irvine, Department of Earth System Sciences, Irvine, California, USA
[7]Jet Propulsion Laboratory, Pasadena, California, USA
[8]Alfred Wegener Institute for Polar and Marine Research, Columbusstrasse, Bremerhaven,
Germany

**A new bed elevation
dataset for Greenland**

J. A. Griggs et al.

Title Page

Abstract	Introduction
Conclusions	References
Tables	Figures

|◀ | ▶|
◀ | ▶
Back | Close

Full Screen / Esc

Printer-friendly Version

Interactive Discussion

A new bed elevation dataset for Greenland

J. A. Griggs et al.

Abstract

We present a new bed elevation dataset for Greenland derived from a combination of multiple airborne ice thickness surveys undertaken between the 1970s and 2011. Around 344 000 line kilometres of airborne data were used, with the majority of this having been collected since the year 2000, when the last comprehensive compilation was undertaken. The airborne data were combined with satellite-derived elevations for non glaciated terrain to produce a consistent bed digital elevation model (DEM) over the entire island including across the glaciated/ice free boundary. The DEM was extended to the continental margin with the aid of bathymetric data, primarily from a compilation for the Arctic. Ice shelf thickness was determined where a floating tongue exists, in particular in the north. The across-track spacing between flight lines warranted interpolation at 1 km postings near the ice sheet margin and 2.5 km in the interior. Grids of ice surface elevation, error estimates for the DEM, ice thickness and data sampling density were also produced alongside a mask of land/ocean/grounded ice/floating ice. Errors in bed elevation range from a minimum of ±6 m to about ±200 m, as a function of distance from an observation and local topographic variability. A comparison with the compilation published in 2001 highlights the improvement in resolution afforded by the new data sets, particularly along the ice sheet margin, where ice velocity is highest and changes most marked. We use the new bed and surface DEMs to calculate the hydraulic potential for subglacial flow and present the large scale pattern of water routing. We estimate that the volume of ice included in our land/ice mask would raise eustatic sea level by 7.36 m, excluding any solid earth effects that would take place during ice sheet decay.

1 Introduction

The bed elevation and ice thickness of the Greenland Ice Sheet are important boundary conditions for numerical modelling. Surface ice velocity is roughly proportional to

A new bed elevation dataset for Greenland

J. A. Griggs et al.

the fourth power of ice thickness and errors in the latter can, therefore, introduce substantial errors in estimated velocities for the present-day or future evolution of the ice sheet. Bed and surface geometry can be used to determine hydraulic potential and, hence, subglacial hydrological pathways (e.g. Wright et al., 2008), while elucidating subglacial topography can also provide insights on the origin and genesis landforms at the bed (e.g. Ferraccioli et al., 2011). For these and other reasons, a large number of airborne field campaigns have been deployed over Greenland during the last decade with a key objective of obtaining ice thickness measurements. The last major compilation of these data for deriving bed elevations was undertaken more than a decade ago (Bamber et al., 2001b) and did not, therefore, include these more recent and extensive field campaigns. In particular, in recent years there has been a focus on acquiring data over the fast-flowing outlet glaciers that fringe the margins of the ice sheet and which are responsible, in part, for the recent acceleration in mass loss observed on the Greenland Ice Sheet (van den Broeke et al., 2009; Howat et al., 2011; Howat and Eddy, 2011). It is now well established that some of these marine-terminating outlet glaciers can respond rapidly, and with large amplitude, to changes in their boundary conditions and, as a consequence, attention has been focussed on modelling their past (Nick et al., 2009) and future behaviour (Nick et al., 2012). For such applications, accurate basal geometry is a critical component for determining rates of grounding-line migration and potential pinning points (Favier et al., 2012). Here, we take an approach that is aimed at maximising the resolution and utility of the basal topography in these key, marginal sectors of the ice sheet: areas that are often challenging for conventional ice penetrating radar (IPR) systems. As a consequence, we employ a range of techniques for improving the bed representation in these areas and interpolate the data at two different resolutions, which are then merged into a single product. This product is intended to be dynamic such that, as new data become available, they will be incorporated in new releases. This paper describes the methods used, and presents the first release of the products.

2 Datasets

2.1 Airborne datasets

In contrast to the previous compilation (Bamber et al., 2001b), bed elevation is the interpolated parameter rather than ice thickness, which is derived from the bed and surface elevation. This means that the bed elevation varies smoothly and realistically across the land/glaciated boundary. To determine the bed elevation, data from a number of airborne IPR missions have been collated. At present, we have collated data from seven sources, each of which is described below and detailed in Table 1. Figure 1 shows the spatial distribution of the different data sources.

2.1.1 Center for remote sensing of ice sheets (CReSIS)

The majority of the data included in this compilation are from a series of instruments developed and flown by CReSIS at the University of Kansas (Gogineni et al., 2001). These data were collected between 1993 and 2009 with the 1993–1999 data being identical to that used previously (Bamber et al., 2001b). Between 1993 and 2002, data were acquired by the Improved Coherent Radar Depth Sounder (ICoRDS). Between 2003 and 2005 the Advanced Coherent Radar Depth Sounder (ACoRDS), between 2006 and 2009, the Multi-Channel Radar Depth Sounder (MCRDS), and since 2010, the Multi-channel Coherent Radar Depth Sounder (MCoRDS) were flown. Since 1999, 96 % more data were available compared with the previous compilation. Since 2006, more time was concentrated on focused campaigns with dense grids over individual outlet glaciers that have changed the most.

The MCoRDS instrument is operated over the 180–210 MHz frequency range with a 10–30 MHz adjustable bandwidth and multiple receivers developed for airborne sounding and imaging of ice sheets. Multiple receivers allow cross-track surface clutter to be suppressed so that relatively weak ice-bed echoes can be retrieved. MCoRDS has been flown on the NASA P-3 and DC-8. Aircraft navigation was from kinematic

GPS and a precision laser altimeter was regularly mounted coincidentally. Using ice core sites, vertical accuracy is estimated to be ±10 m (Gogineni et al., 2001), but it is worse in areas where the ice bottom is ambiguous (e.g. in hilly terrain or when clutter obscures the desired basal return) and larger cross-over errors are commonly seen in these regions. Level 2 data containing location and ice thickness are available from CReSIS. Level 1b geolocated radar echo strength profile images were used only to verify the removal of some data which appeared to be unphysical.

In a region close to the outlet of Jakobshavn Isbrae, CReSIS produced a 125 m resolution bed DEM. This includes all data collected by them in the region between 1997 and 2007. This grid was used in place of the original CReSIS data as they reprocessed all the data in the channel and collocated the data with coincidental lidar surface elevations. Additionally, they included ASTER data in bare rock areas and fjord soundings to complement the airborne data.

2.1.2 Operation IceBridge (OIB)

Since 2010, the MCoRDS instrument has flown as part of the NASA Operation Ice-Bridge (OIB) programme (Studinger et al., 2010). OIB is designed to provide airborne data to fill the gap between the end of the ICESat satellite record in 2009 and the launch of ICESat-2 which is scheduled for 2016. MCoRDS operates on all flights where ice thickness measurements can be retrieved. Several of the existing dense grids over rapidly changing outlets were flown as well as grids over new outlets and flowlines of many more glaciers. These data significantly improve coverage particularly where narrow, fast outlets were previously unsurveyed around the north and south-west coasts of Greenland.

2.1.3 Alfred-Wegener-Institut (AWI)

The AWI instrument is capable of penetrating 4 km of ice with better than 50 m vertical accuracy and 3.25 m along-track resolution (Nixdorf et al., 1999). It operated at

150 MHz transmitting bursts of 60 ns and 600 ns duration. In earlier years a combination of GPS and inertial navigation was used and, since 1997, differential GPS was employed. Horizontal navigation errors are up to ±100 m. Data were collected in 1996–1999, 2004 and 2010, operating out of the NGRIP camp site in Central Greenland (Nixdorf and Goktas, 2001) and from coastal airstrips at Station Nord (Meyer et al., 1999) and Qaanaaq. This gives dense coverage in Central Northern Greenland (Fig. 1).

2.1.4 Warm Ice Sounding Explorer (WISE)

WISE is an airborne sounder designed to measure ice thickness in areas of warm and fractured ice. It is based on the MARSIS planetary sounder used on Mars. It operates at a 2.5 MHz centre frequency with a monopole antenna with navigation using conventional GPS. It was operated by the NASA Jet Propulsion Laboratory (JPL) on an Air Greenland Twin Otter as an IPY deployment on the NASA Twin Otter. Data were collected in 2008, 2009 and 2010 in marginal areas. WISE is the only radar that has returned bed echoes in Southwest Greenland.

2.1.5 Pathfinder Advanced Radar Ice Sounder (PARIS)

PARIS flew in 2009 and was operated by Johns Hopkins University on an Operation Ice Bridge flight (Raney, 2010). PARIS successfully demonstrated high altitude soundings with a delay Doppler design. The along track resolution of the data was 250 m with a vertical accuracy of 12.5 m.

2.1.6 High-Capability RadarSounder (HICARS)

HICARS is operated by the University of Texas Institute for Geophysics and JPL (Peters et al., 2005, 2007). It is a 60 MHz phase coherent pulsed radar with a 15 MHz bandwidth. It has flown extensively in Antarctica including surveys over the Thwaites Glacier catchment and surveys of large sectors of East Antarctica (Wright et al., 2012).

A new bed elevation dataset for Greenland

J. A. Griggs et al.

Title Page

Abstract	Introduction
Conclusions	References
Tables	Figures

◄◄ ►►

◄ ►

Back Close

Full Screen / Esc

Printer-friendly Version

Interactive Discussion

New algorithms employed with HICARS allow a horizontal resolution of less than 5 m and vertical resolution of ±10 m.

2.1.7 Technical University of Denmark (TUD)

A small amount of data is included which were collected in the 1970's by the TUD using a 60 MHz echo sounder, analogue recording and inertial navigation. The quality of these data is, in general, poorer than the more recent data so they are only used when there are no other data sources within 50 km (Fig. 1) (Bamber et al., 2001b).

2.2 Surface elevations

All the airborne data were provided as ice thickness measurements but we require bed elevation. Therefore, a surface elevation estimate is needed. For some of the CReSIS and OIB campaigns, the flights also operated the NASA Airborne Topographic Mapper (ATM): an airborne laser altimeter. ATM scans the surface and is resampled to a horizontal spacing of 50 m with data averaged into 80 m diameter platelets. ATM was not always available and so our secondary source of surface elevations was from a DEM of the whole of Greenland. The surface DEM used was produced as part of the Greenland Ice Mapping Project (GIMP). It has a horizontal resolution of 90 m and is a multi-sensor DEM derived from data collected between 2000 and 2009. This DEM was created from MODIS, AVHRR, ASTER, SPOT and RADARSAT datasets merged with the ASTER GDEM and the Bamber et al. (2001a) DEM vertically co-registered using ICESat data. Validation against ICESat data, indicated vertical errors of ±5 m on the ice sheet and ±7 m for the unglaciated margins (Howat, personal communication, 2010).

2.3 Bathymetry

Numerical modelling over long timescales, such as glacial-interglacial cycles, or spinning up the thermodynamics in an ice sheet model requires basal geometry that extends out to the continental shelf: i.e. as far the maximum glacial extent which can

A new bed elevation dataset for Greenland

J. A. Griggs et al.

reach to the shelf edge several hundred kilometres from the present-day ice limit under full-glacial conditions (Evans et al., 2009; Dowdeswell et al., 2010; Cofaigh et al., 2012). To achieve this requires inclusion of bathymetric data. Here we used the International Bathymetric Chart of the Arctic Ocean v2 (Jakobsson et al., 2008). This is

5 an interpolation of various bathymetric data from the entire Arctic Ocean and a DEM for Greenland, Ellesmere Island and Iceland. It was supplemented with additional data from soundings in the Jakobshavn fjord, which were included in the CReSIS Jakobshavn grid described above. Other changes to this dataset, and the reasons for these changes, are as described in Sect. 3.2.3.

10   3   Methods

All the airborne data were transformed onto a polar stereographic projection with standard parallel at 71° N and a central meridian of 39° W. All invalid data, as defined by the instrument teams, all data outside Greenland, and all data with ice thickness less than 0 m were removed. Rather than interpolating ice thickness, which has a discontinuity at

15 the ice sheet margin, we interpolate bed elevation, as this varies smoothly across the ice edge. By combining the high resolution surface topography with the bed data we can create a more realistic ice margin. Where CReSIS thickness data were acquired within 2 days and within 1 km of an ATM surface elevation, the ATM estimate is used to convert to bed elevation. For 18 % of ice thickness estimates from CReSIS when ATM

20 was also flown, no surface elevation estimate was recorded. In those cases, and for all other datasets, the GIMP DEM was used.

To interpolate the bed, it is necessary to delineate glaciated and ice-free terrain. A land surface mask was created by merging a number of data sources. The coastline of Greenland was smoothed to a 1 km resolution from the Danish Ministry of Environ-

25 ment (formerly KMS) 1 : 2 500 000 scale vector maps of the coast. The Canadian Arctic and Iceland were separated from the Greenland coast by identifying distinct polygons. The ice sheet and periphery ice caps were identified using a binary mask (Howat and

A new bed elevation dataset for Greenland

J. A. Griggs et al.

Negrete, 2012) produced from a combination of Landsat 7 panchromatic band imagery from July–September 1999–2001 and RADARSAT-1 SAR amplitude images from autumn 2000. Data were provided at 180 m horizontal spacing and reprojected onto the polar stereographic grid at 1 km resolution. Gridboxes with over 50 % ice cover were considered to be ice sheet/ice cap. Ice shelves were categorized separately from the rest of the ice sheet. The existence of an ice shelf was determined by the presence of a grounding line from Interferometric Synthetic Aperture Radar. Grounding lines were provided by Eric Rignot (JPL) and are a sub-set of those previously published (Rignot et al., 1997). The ice shelf front was determined by a number of means. In areas with ATM coverage, the ice front was located by a step in the elevations. This was confirmed by ice front locations from the KMS maps. In the absence of ATM data, the KMS ice fronts were used alone. On Storstrommen and Ostenfeld glaciers, no front was present in maps or ATM data but InSAR confirmed the presence of an ice shelf. In these cases, a small shelf was added based on Google Earth imagery. No attempt was made to determine the bed elevation of peripheral glaciers where no thickness data exist (see Fig. 1) and, in this case, it is the glacier surface elevation that is obtained, if resolved at all at 1 km.

3.1 Data editing

The data were gridded with 5 km postings and a 3 standard deviation filter was applied twice to remove elevation outliers. This removed 0.3 % of datapoints. Visual inspection indicated that the filter had removed noisy data but a small number of anomalous measurements remained. These were tracks which were not picking the ice/bed interface but appeared to be tracking an internal layer. A coarse filter was applied whereby a data point was removed if the bed elevation was more than 500 m different from the previous estimate (Bamber et al., 2001b). This was only applied in areas where there was previous data coverage and not in areas with large relief or areas of high surface velocity ($> 100\,\mathrm{m\,yr}^{-1}$). Visual inspection also led to the removal of several other tracks from the CReSIS data after examination of the echograms. In all, 98.6 % of the data

from the various campaigns were determined to be over ice and of sufficient quality to be included.

3.2 Interpolation

All data which passed the quality checks were locally averaged into a quasi-regular
1 km and 2.5 km resolution grid, which reduced the disparity in along and across track spacing of the data. The resolution of the two grids was chosen based on the data density. For surface elevations below 2000 m, a 1 km resolution posting results in 29 % of grid points containing data. At higher elevations, data are sparser, bed gradients are smaller and a lower resolution is appropriate. At 2.5 km posting, 33 % of grid points
above 2000 m surface elevation contain data. In areas identified by the mask as being unglaciated, surface elevation data from the GIMP DEM were included in the quasi regular grid.

The 1 and 2.5 km quasi-regular grids were interpolated to regular grids using ordinary kriging. The GSLIB library (Deutsch and Journel, 1997) was used to calculate variograms. Separate variograms above and below 2000 m surface elevation were calculated due to the differing volumes of data and differing underlying topography. In the ice sheet interior, the bed is smoother and flatter. Closer to the ice margin, the bed is rougher and incised with deep troughs that are occupied by fast flowing outlet glaciers. An exponential function was fitted to the first 100 km of each variogram using a non-linear least squares scheme. These variograms were used to interpolate the quasi-regular grids using a nugget of 50 m to take account of uncertainty in the airborne data. A maximum of 50 quasi-regular grid points were considered and the maximum search radius was set to 100 km so that a result was obtained everywhere.

The 2.5 km grid was bilinearly interpolated to 1 km resolution. This avoids interpolation artefacts produced by interpolating sparse data at 1 km while creating a grid at one horizontal posting, which affords a simpler data structure compared with a multi-resolution or nested grid. The two grids were combined using the 1 km resolution grid at all surface elevations lower than 2000 m and in the Petermann, Jakobshavn,

A new bed elevation dataset for Greenland

J. A. Griggs et al.

Kangerdlussuaq and Helheim outlet glaciers (as these contain dense grids of flight lines) and the bilinearly interpolated 2.5 km resolution grid elsewhere. The merging was done using a Hermite basis function of width 20 km across the boundary.

Ice thickness was derived by subtracting the bed from the GIMP DEM for every grid point defined as ice covered in the mask. The minimum ice thickness at the margin was set to 50 m. Wherever the thickness was less than this, the bed was lowered to be 50 m below the GIMP surface elevation. This is necessary because thickness data around much of the margin of the ice sheet does not exist (Fig. 1) and therefore, subglacial bed elevations cannot be determined directly in these areas but must be interpolated close to a discontinuity in thickness and surface elevation.

3.2.1 Ice shelves

Nine ice shelves are present around the Greenland Ice Sheet according to our land mask. The surface elevation for most of each ice shelf area was found by combining all GIMP, ATM and airborne ice thicknesses measurements converted to surface elevation using hydrostatic equilibrium. Some ice shelf gridpoints contain no elevation data from any source, in which case, nearest neighbour interpolation from other ice shelf elevations was used. For Nioghalvfjerdsbrae and Zachariae Isstrom, only ATM and airborne elevations were used as GIMP elevations were not in agreement with the other data sources. The airborne ice thicknesses were converted to surface elevations to increase data coverage.

Ice shelf thickness was calculated from surface elevation using hydrostatic equilibrium (see Griggs and Bamber, 2011 for a full description of the method). A constant firn density correction of 10 m was used throughout. An ocean water density of 1027 kg m^{-3} and an ice density of 917 kg m^{-3} were chosen. The same parameters were used to convert the airborne ice thicknesses to surface elevations and back again, having no net effect on basal elevations but increasing data coverage. In areas where the surface elevation is less than 10 m above sea level, and ice thickness would be calculated to be negative, surface elevations were interpolated from thicker neighbouring datapoints. In

areas where hydrostatic equilibrium is invalid such as the shear margin on Petermann Glacier, ice thickness was smoothed from surrounding datapoints.

3.2.2 Mass conservation

In many areas, there were no airborne data within a few kilometres of glacier termini. If there are unglaciated regions closer to the terminus than the closest airborne data, they dominate the interpolated elevation at the terminus, artificially raising the bed elevations. This was corrected for in two ways. In four areas, we had an airborne survey line which crossed the fast-flowing region of the outlet. In these cases, we took the bed elevations at the airborne data points along with the known velocity (Joughin et al., 2010) and the 30-yr average modelled surface mass balance (Ettema et al., 2009) and calculated the expected bed elevation based on the principle of mass conservation. The direction of flow of the ice from the location of the airborne data to the terminus was determined by the direction of the velocity vector.

Figure 2 shows the result of correcting the bed elevations using this method for one outlet. In (a) the original elevations are shown and (b) shows the bed after the application of the technique. A region of 7 km length is altered from the position of an airborne track inland, following the region of faster flowing ice as shown in Fig. 2c. It is clear that after this change, thick ice is now able to flow along the outlet where previously a ridge was mapped due to the inclusion of measurements of unglaciated terrain closer to the terminus than legitimate ice thickness data.

In a number of other locations, the same situation arises but either there are no velocity measurements, the velocity vectors make the ice flow out of the region of fast flow, unsurveyed tributaries join the main flow oceanward of the airborne data, or the airborne measurements do not cross the entire fast flow channel. In these cases, the mass conservation scheme cannot be readily implemented and instead, linear interpolation was used to remove the artificial ridges at the terminus. In all cases where data were changed from the original interpolated values, a mask is provided which notes the change made, the reason and the original interpolated value.

3.2.3 Bathymetry interpolation

The interpolated bed elevations were merged with the known bathymetry of the fjords and oceans around Greenland (Jakobsson et al., 2008). A smoothing distance of 3 km was used on the ocean-ward side of the coastline to merge the two datasets. No smoothing was used in the south-west where the coastline consists of many narrow fjords. Any smoothing zone in this area would result in the fjords being completely removed. In a number of areas the bathymetry is not well known and IBCAO does not contain any observations (see figure here: http://www.ngdc.noaa.gov/mgg/bathymetry/arctic/images/IBCAO-sources.jpg). In some of those areas, our coastal bed elevations suggest that the IBCAO bathymetry is significantly too high. In a number of fjords, including Jakobshavn and Petermann, the bathymetry data are particularly high and appear to follow the ice surface rather than the fjord bottom. In Jakobshavn fjord, we replaced the IBCAO bathymetry with that from the CReSIS grid described in Sect. 2.1.1. In other areas, no bathymetric data were available and the IBCAO interpolation contains a fjord which is much shallower than the bed elevation at the grounding line or glacier terminus. For example at Hagen Brae, the fjord just oceanward of the grounding line was 200 m shallower than the bedrock elevation at the grounding line. To ensure realistic ice flow pathways, we lowered the bathymetry in regions affected in this way to create a smooth surface without a discontinuity at the land/ocean margin. We have not included any new bathymetric data as this is beyond the scope of this study. In the affected areas, we interpolated between the grounding line/glacier terminus and beyond the fjord mouth using triangulation. The results were smoothed over 2 km around the triangulated values. End points for the interpolation were chosen to ensure that ice flows out of the fjord. The approach is somewhat subjective and results depend upon the choice of endpoints. A mask is provided with the data which shows where the bathymetry has been changed in this manner.

Since the data described here were processed an updated IBCAO (v3) has been released (Jakobsson et al., 2012). These data will be incorporated into future releases.

Title Page

Abstract | Introduction

Conclusions | References

Tables | Figures

◄ | ►

◄ | ►

Back | Close

Full Screen / Esc

Printer-friendly Version

Interactive Discussion

However, the major update close to the Greenland coast is in the fjord geometry around Jakobshavn where we have replaced the IBCAO v2 values with CReSIS processed sounding data. Most other areas where IBCAO v2 was altered would still need to be altered if IBCAO v3 had been used and we believe, therefore that the newer bathymetry provides minimal improvement for this particular application.

4   Results and discussion

The final bed DEM was referenced to the EIGEN-GL04C geoid (Forste et al., 2008) and is shown in Fig. 3. Alongside this, we also produced grids of ice thickness, surface elevation, error maps of surface and bed elevation, the land surface mask, the geoid-ellipsoid separation, a mask showing changes made to the bed elevation post-interpolation, the bed elevation and ice thickness without any intervention, a mask showing the data sources used for the ice shelves and a grid of the number of airborne data per grid-point. The data includes features which were not visible in previous compilations as well as improving the representation of features previously observed. The improvement is most noticeable in areas of relatively high relief close to the ice margin and, in particular, where dense grids were flown (Fig. 1, and Supplement Fig. S1). Under Jakobshavn (black box on Fig. 3), there is a dendritic, channel system extending for about 325 km from the current grounding line into the interior almost as far as the ice divide (Hoch et al., 2011). It seems likely that this is a paleo-fluvial feature that predates ice cover in Greenland and is clearly an important control on the ice dynamics of the basin. The presence of a deep trough extending into the interior has been previously reported, based on SAR processing of MCoRDS data (Hoch et al., 2011).

We make a direct comparison between the new bed DEM and the one from the previous compilation (Bamber et al., 2001b) in two regions to illustrate the improvements made. Figure 4a shows the Jakobshavn region in the new dataset (see black box in Fig. 3 for location) and (b) shows the same region in the older dataset. First, it is apparent that the true resolution (as opposed to the grid spacing) of the new DEM

is significantly improved throughout the region, better characterising the undulating sub-glacial mountains to the north of the trough between 0–100 km along the x-axis and 120–200 km along the y-axis. Secondly, the deep trough under the main fjord is present. The previous compilation showed almost no evidence of this trough due to (i) a lack of bed returns in this area and (ii) the resolution of the older grid at 5 km. The width of the trough in the new DEM is 3–4 km. The region of fastest flow coincides fairly well with the location of the deepest ice (Fig. 4c). The trough in the new DEM is 1366 m below sea level at its deepest point compared to a maximum depth over the entire region of 556 m below sea level in the older dataset. The main trough of Jakobshavn Isbrae is not continuous in the new dataset, disappearing around 100 km on the x-axis and reappearing at about 140 km on the x-axis. This does not demonstrate that the trough is discontinuous, but only that there are insufficient data to confirm its presence or otherwise in this region.

Figure 4d and e show a similar comparison for a 200 km by 500 km area along the north-west coast of Greenland (red box in Fig. 3). In the older DEM, there is some evidence of bed troughs but they are wide and not well aligned with the areas of fast flow seen in Fig. 4f. Figure 4d shows numerous troughs, all aligned with areas of fast flow. The wide unconstrained minimum seen in Fig. 4e at a depth of 438 m below sea level is now seen as a deep, narrow trough under a region of fast flow with a maximum depth of 1219 m below sea level. This improvement is due mainly to the increased data coverage and to a lesser extent the higher resolution of the DEM. Similar comparisons can be made elsewhere and the full fidelity of the dataset becomes apparent when examining smaller regions of a few hundred kilometres in extent.

4.1 Hydraulic potential

Important information about potential water-flow routing beneath the ice sheet can be deduced from high quality surface and bed topography (e.g. Wright et al., 2008). Here we use the theory developed by Shreve (1972) to calculate the subglacial hydraulic pressure potential and the flow paths that follow the gradients in this potential. Figure 5

shows the major subglacial flow paths colour coded, darker colours indicating a larger catchment contributing to the flow. In the main the flow paths follow the direction of ice flow. For a given thickness of water per unit area, the colour coding provides a measure of the volume of water associated with a particular flow path which is largely controlled by the size of the ice surface catchment area for a given outlet glacier. Not surprisingly and similarly to a previous analysis (Lewis and Smith, 2009), glaciers such as Helheim, Kangerdlussuaq and Jakobshavn Isbrae, which have large catchments, have the potential for substantial subglacial drainage beneath their main trunks. The Northeast Greenland ice stream is also a major conduit for subglacial water flow and it is interesting to note that high geothermal activity has been proposed to produce a large volume of water near the onset of this feature (Fahnestock et al., 2001). Combined with modelled estimates for basal melt and surface percolation to the bed, the flow routing shown in Fig. 5 can be used to estimate subglacial water discharge at the ice margin and compared, for example, with field-based estimates (DeFoor et al., 2011).

4.2 Error assessment

For most applications, a reliable estimate of the uncertainty in the DEM is essential. To determine the total error we considered (i) the random error in the thickness observation and (ii) the impact of interpolation. The former was assessed from a track-to-track difference analysis of the data (a combination of repeat track and quasi-crossover differences). We consider the differences between any two measurements obtained at different times within a 50 m area. This has the advantage of including along track differences in cases where aircraft fly repeat tracks in subsequent seasons as well as crossovers. In total, 24.1 million differences were calculated. The data were split by campaign to calculate both inter and intra-campaign differences. These data, strictly, only provide information on repeatability and not systematic biases but, because we are considering inter-campaign differences, we believe that biases due, for example, to timing, navigation or radar calibration errors, will be captured in this analysis. Only

Printer-friendly Version

Interactive Discussion

biases common across all campaigns (such as a common error in the radio wave velocity in ice used) will not be seen.

Table 2 summarises the differences for each set of campaigns grouped by instrument and/or institute. Figure 6a shows the histogram of differences, which has a Gaussian distribution with a bias close to zero. We estimate the random error as $1/\sqrt{2}$ (because a difference contains two observations) of the standard deviation of the inter-campaign difference of the nearest data to a grid point. In the case of TUD data, where there are no differences, we use the standard deviation of all inter- and intra- campaign values.

Next we consider the error due to interpolation. This increases with distance from an observation but is also a function of the properties of the underlying surface. We estimate this uncertainty using a bootstrap approach for two classes of bed topography: coastal and interior. We took the CReSIS data from the 2000s in two locations that are broadly representative of these two categories: first, the basin of the Petermann Glacier being representative of coastal, high relief and, secondly, a 550 by 1200 km region centred on Summit, being representative of the interior. In both areas, we repeated the interpolation while removing a random portion (of up to 90 %) of data. The difference between the interpolated and observed elevation as a function of distance was used as a measure of the interpolation error. The standard deviation of these differences for the two areas is shown in Fig. 6b. A line with correlations of $r^2 = 0.92$ for the Petermann basin and $r^2 = 0.80$ for the central plateau was fitted to the differences. This fit was used to determine the error due to interpolation as a function of distance. Areas with surface elevation below 2000 m were assigned as "coastal" and areas above this elevation as "interior".

The two sources of error were combined in quadrature to produce a map of the uncertainty in the bed elevation (Fig. 7). As expected the error increases significantly with distance from an observation and the largest errors occur in coastal regions where extrapolation, rather than interpolation, was needed. For the peripheral ice caps where, in most cases, there are no airborne data, the bed elevation is poorly constrained and these areas are included only for completeness. Better estimates of the ice thickness

in these areas could be estimated using an ice-surface area/volume scaling approach (Bahr et al., 1997).

5   Conclusions

A large volume of high quality new data have become available since the last comprehensive dataset of ice thickness in Greenland was compiled (Bamber et al., 2001b). We improve on the earlier compilation in several respects. Most importantly, we have included extensive new data sets acquired by several different groups over the last decade. A significant effort has been made, during this period, to sound the bed of fast-flowing outlet glaciers which were either missed or proved challenging targets for the previous generation of IPR systems due to high attenuation and clutter. These new datasets also provide improved coverage of the, previously, sparsely surveyed interior. The greater coverage and dense network of flightlines in many coastal areas (Fig. 1 and Supplement Fig. S1) supports a grid spacing of 1 km, five times higher than the previous compilation. As a consequence, many basal features, in particular basal troughs containing outlet glaciers, are now resolved in the bed topography. In the ice sheet interior, flight lines are less dense but the topography is generally smoother and, therefore, a coarser resolution captures the salient features. For convenience, the bed DEM is provided at a single posting of 1 km alongside a grid indicating whether the value is interpolated or based on observation. An error map for the DEM was also calculated and indicates areas where additional data would be particularly useful. The estimated volume of the ice sheet is 2.96×10^6 km^3 compared with 2.93×10^6 km^3 obtained previously (Bamber et al., 2001b). 1.5 % of the ice sheet bed is below sea level and, accounting for this and the thickness of the firn layer but excluding any glacio-isostatic adjustment, we estimate that the ice sheet has the potential to raise eustatic sea level by 7.36 m were it all to melt.

The data presented here represent a major advance in our knowledge of the topography of the bedrock of Greenland. However, there are several areas where data are

currently lacking such as along much of the central and north eastern margins of the ice sheet (Fig. S1). While the interior of Greenland is relatively smooth, there are still many areas where the distance to the closest observation is greater than 50 km, resulting in uncertainties in bed elevation of about ±110 m. In general, interpolation techniques will underestimate ice thickness in sparsely covered regions limiting the ability of numerical models to replicate rapid changes in these regions. Recent results suggest reduced uncertainty and significantly increased spatial detail can be obtained from radar tomography (Jezek et al., 2011; Paden et al., 2010). Wide application of these techniques could significantly improve current mapping by decreasing the amount of interpolation needed over deeply incised outlet glaciers. Bathymetry in front of the glaciers and beneath ice shelves is currently poorly characterised in some areas and non existent in most. This is a major gap in our current knowledge and requires further effort by the community. New data are being acquired over Greenland each year and we intend to issue new releases of the products when sufficient new data become available. The next release will include, as a minimum, OIB and other IPR data collected in 2012 as well as IBCAO v3. The complete set of grids, metadata and documentation are available in netcdf format from the corresponding author (JLB). Users will be notified of new releases as they become available.

Supplementary material related to this article is available online at: http://www.the-cryosphere-discuss.net/6/4829/2012/tcd-6-4829-2012-supplement. pdf.

References

Bahr, D. B., Meier, M. F., and Peckham, S. D.: The physical basis of glacier volume-area scaling, J. Geophys. Res-Sol. Ea., 102, 20355–20362, doi:10.1029/97jb01696, 1997.

Bamber, J., Ekholm, S., and Krabill, W.: A new, high-resolution digital elevation model of Greenland fully validated with airborne laser altimeter data, J. Geophys. Res., 106, 6733–6745, 2001a.

Bamber, J. L., Layberry, R. L., and Gogineni, S.: A new ice thickness and bed data set for the Greenland ice sheet 1. Measurement, data reduction, and errors, J. Geophys. Res.-Atmos., 106, 33773–33780, 2001b.

Cofaigh, C. O., Dowdeswell, J. A., Jennings, A. E., Hogan, K. A., Kilfeather, A. A., Hiemstra, J. F., Noormets, R., Evans, J., McCarthy, D. J., Andrews, J. T., Lloyd, J. M., and Moros, M.: An extensive and dynamic ice sheet on the West Greenland shelf during the last glacial cycle, Geology, in press., 2012.

DeFoor, W., Person, M., Larsen, H. C., Lizarralde, D., Cohen, D., and Dugan, B.: Ice sheet-derived submarine groundwater discharge on Greenland's continental shelf, Water Resour. Res., 47, W07549, doi:10.1029/2011wr010536, 2011.

Deutsch, C. L. and Journel, A. G.: GSLI B. Geostatistical software library and user's guide, 2nd edn., Oxford University Press, Oxford, 369 pp., 1997.

Dowdeswell, J. A., Evans, J., and Cofaigh, C. O.: Submarine landforms and shallow acoustic stratigraphy of a 400 km-long fjord-shelf-slope transect, Kangerlussuaq margin, East Greenland, Quaternary Sci. Rev., 29, 3359–3369, doi:10.1016/j.quascirev.2010.06.006, 2010.

Ettema, J., van den Broeke, M. R., van Meijgaard, E., van de Berg, W. J., Bamber, J. L., Box, J. E., and Bales, R. C.: Higher surface mass balance of the Greenland ice sheet revealed by high-resolution climate modeling, Geophys. Res. Lett 36, L12501, doi:10.1029/2009gl038110, 2009.

Evans, J., Cofaigh, C. O., Dowdeswell, J. A., and Wadhams, P.: Marine geophysical evidence for former expansion and flow of the Greenland Ice Sheet across the North-east Greenland continental shelf, J. Quaternary Sci., 24, 279–293, doi:10.1002/jqs.1231, 2009.

Fahnestock, M., Abdalati, W., Joughin, I., Brozena, J., and Gogineni, P.: High geothermal heat row, basal melt, and the origin of rapid ice how in Central Greenland, Science, 294, 2338–2342, doi:10.1126/science.1065370, 2001.

A new bed elevation dataset for Greenland

J. A. Griggs et al.

Title Page

Abstract	Introduction
Conclusions	References
Tables	Figures

◀ | ▶|

◀ | ▶

Back | Close

Full Screen / Esc

Printer-friendly Version

Interactive Discussion

Favier, L., Gagliardini, O., Durand, G., and Zwinger, T.: A three-dimensional full Stokes model of the grounding line dynamics: effect of a pinning point beneath the ice shelf, The Cryosphere, 6, 101–112, doi:10.5194/tc-6-101-2012, 2012.

Ferraccioli, F., Finn, C. A., Jordan, T. A., Bell, R. E., Anderson, L. M., and Damaske, D.: East Antarctic rifting triggers uplift of the Gamburtsev Mountains, Nature, 479, 388–394, doi:10.1038/nature10566, 2011.

Forste, C., Schmidt, R., Stubenvoll, R., Flechtner, F., Meyer, U., Konig, R., Neumayer, H., Biancale, R., Lemoine, J. M., Bruinsma, S., Loyer, S., Barthelmes, F., and Esselborn, S.: The GeoForschungsZentrum Potsdam/Groupe de Recherche de Geodesie Spatiale satellite-only and combined gravity field models: EIGEN-GL04S1 and EIGEN-GL04C, J. Geodesy, 82, 331–346, 2008.

Gogineni, S., Tammana, D., Braaten, D., Leuschen, C., Akins, T., Legarsky, J., Kanagaratnam, P., Stiles, J., Allen, C., and Jezek, K.: Coherent radar ice thickness measurements over the Greenland ice sheet, J. Geophys. Res-Atmos., 106, 33761–33772, 2001.

Griggs, J. A. and Bamber, J. L.: Antarctic ice-shelf thickness from satellite radar altimetry, J. Glaciol, 57, 485–498, 2011.

Hoch, A. M., Velez, J. A., Tsoflias, G. P., Stearns, L. A., Van der Veen, C. J., and IEEE: Multichannel Cooherent Radar Depth Sounding of Jakobshavn Isbrae and its Catchment, in: 2011 IEEE Radar Conference, IEEE National Radar Conference Proceedings, IEEE, New York, 1135–1137, 2011.

Howat, I. M., Ahn, Y., Joughin, I., van den Broeke, M. R., Lenaerts, J. T. M., and Smith, B.: Mass balance of Greenland's three largest outlet glaciers, 2000–2010, Geophys. Res. Lett., 38, L12501, doi:10.1029/2011gl047565, 2011.

Howat, I. M. and Eddy, A.: Multi-decadal retreat of Greenland's marine-terminating glaciers, J. Glaciol., 57, 389–396, 2011.

Jakobsson, M., Macnab, R., Mayer, L., Anderson, R., Edwards, M., Hatzky, J., Schenke, H. W., and Johnson, P.: An improved bathymetric portrayal of the Arctic Ocean: implications for ocean modeling and geological, geophysical and oceanographic analyses, Geophys. Res. Lett., 35, L07602, doi:10.1029/2008gl033520, 2008.

Jakobsson, M., Mayer, L., Coakley, B., Dowdeswell, J. A., Forbes, S., Fridman, B., Hodnesdal, H., Noormets, R., Pedersen, R., Rebesco, M., Schenke, H. W., Zarayskaya, Y., Accettella, D., Armstrong, A., Anderson, R. M., Bienhoff, P., Camerlenghi, A., Church, I., Edwards, M., Gardner, J. V., Hall, J. K., Hell, B., Hestvik, O., Kristoffersen, Y., Marcussen, C.,

A new bed elevation dataset for Greenland

J. A. Griggs et al.

Title Page

Abstract	Introduction
Conclusions	References
Tables	Figures

◄◄ | ►►

◄ | ►

Back | Close

Full Screen / Esc

Printer-friendly Version

Interactive Discussion

Mohammad, R., Mosher, D., Nghiem, S. V., Teresa Pedrosa, M., Travaglini, P. G., and Weatherall, P.: The international bathymetric chart of the Arctic ocean (IBCAO) Version 3.0, Geophys. Res. Lett., 39, L12609, doi:10.1029/2012gl052219, 2012.

Jezek, K., Wu, X. Q., Gogineni, P., Rodriguez, E., Freeman, A., Rodriguez-Morales, F., and Clark, C. D.: Radar images of the bed of the Greenland ice sheet, Geophys. Res. Lett., 38, L01501, doi:10.1029/2010gl045519, 2011.

Joughin, I., Smith, B. E., Howat, I. M., Scambos, T., and Moon, T.: Greenland flow variability from ice-sheet-wide velocity mapping, J. Glaciol., 56, 415–430, 2010.

Lewis, S. M. and Smith, L. C.: Hydrologic drainage of the Greenland ice sheet, Hydrol. Process., 23, 2004–2011, 10.1002/hyp.7343, 2009.

Meyer, U., Damaske, D., Steinhage, D., Nixdorf, U., and Miller, H.: First highlights from NO-GRAM'98 – northern gravity, radio echo sounding and magnetics, Polarforschung, 69, 25–33, 1999.

Nick, F. M., Vieli, A., Howat, I. M., and Joughin, I.: Large-scale changes in Greenland outlet glacier dynamics triggered at the terminus, Nat. Geosci., 2, 110–114, doi:10.1038/ngeo394, 2009.

Nick, F. M., Luckman, A., Vieli, A., Van Der Veen, C. J., Van As, D., Van De Wal, R. S. W., Pattyn, F., Hubbard, A. L., and Floricioiu, D.: The response of Petermann glacier, Greenland, to large calving events, and its future stability in the context of atmospheric and oceanic warming, J. Glaciol., 58, 229–239, doi:10.3189/2012JoG11J242, 2012.

Nixdorf, U. and Goktas, F.: Spatial depth distribution of the subglacial bed and internal layers in the ice around NGRIP, Greenland, derived with airborne RES, J. Appl. Geophys., 47, 175–182, doi:10.1016/s0926-9851(01)00062-3, 2001.

Nixdorf, U., Steinhage, D., Meyer, U., Hempel, L., Jenett, M., Wachs, P., and Miller, H.: The newly developed airborne radio-echo sounding system of the AWI as a glaciological tool, in: Annals of Glaciology, 29, edited by: Jacka, T. H., Int. Glaciological Soc., Cambridge, 231–238, 1999.

Paden, J., Akins, T., Dunson, D., Allen, C., and Gogineni, P.: Ice-sheet bed 3-D tomography, J. Glaciol., 56, 3–11, 2010.

Peters, M. E., Blankenship, D. D., and Morse, D. L.: Analysis techniques for coherent airborne radar sounding: application to West Antarctic ice streams, J. Geophys. Res.-Sol. Ea., 110, B06303, doi:10.1029/2004jb003222, 2005.

A new bed elevation dataset for Greenland

J. A. Griggs et al.

Title Page	
Abstract	Introduction
Conclusions	References
Tables	Figures

◄◄	►►
◄	►
Back	Close

Full Screen / Esc

Printer-friendly Version

Interactive Discussion

Peters, M. E., Blankenship, D. D., Carter, S. P., Kempf, S. D., Young, D. A., and Holt, J. W.: Along-track focusing of airborne radar sounding data from West Antarctica for improving basal reflection analysis and layer detection, IEEE T. Geosci. Remote, 45, 2725–2736, doi:10.1109/tgrs.2007.897416, 2007.

Raney, K.: IceBridge PARIS L2 Ice Thickness, 2009, Boulder, Colorado USA: NASA Distributed Active Archive Center at the National Snow and Ice Data Center, digital media, available at: http://nsidc.org/data/irpar2.html, 2010.

Rignot, E. J., Gogineni, S. P., Krabill, W. B., and Ekholm, S.: North and Northeast Greenland ice discharge from satellite radar interferometry, Science, 276, 934–937, 1997.

Shreve, R. L.: Movement of water in glaciers, J. Glaciol., 11, 205–214, 1972.

Studinger, M., Koenig, L., Martin, S., Sonntag, J., and IEEE: Operation IceBridge: using instrumented aircraft to bridge the observational gap between ICESat and ICESat-2, 2010 IEEE International Geoscience and Remote Sensing Symposium, IEEE, New York, July 25–30, 1918–1919, 2010.

van den Broeke, M., Bamber, J., Ettema, J., Rignot, E., Schrama, E., van de Berg, W. J., van Meijgaard, E., Velicogna, I., and Wouters, B.: Partitioning recent Greenland mass loss, Science, 326, 984–986, doi:10.1126/science.1178176, 2009.

Wright, A. P., Siegert, M. J., Le Brocq, A. M., and Gore, D. B.: High sensitivity of subglacial hydrological pathways in Antarctica to small ice-sheet changes, Geophys. Res. Lett., 35, L17504, doi:10.1029/2008gl034937, 2008.

Wright, A. P., Young, D. A., Roberts, J. L., Schroeder, D. M., Bamber, J. L., Dowdeswell, J. A., Young, N. W., Le Brocq, A. M., Warner, R. C., Payne, A. J., Blankenship, D. D., van Ommen, T. D., and Siegert, M. J.: Evidence of a hydrological connection between the ice divide and ice sheet margin in the Aurora subglacial basin, East Antarctica, J. Geophys. Res.-Earth Surf., 117, F01033, doi:10.1029/2011jf002066, 2012.

Title Page

Abstract | Introduction

Conclusions | References

Tables | Figures

◄ | ►

◄ | ►

Back | Close

Full Screen / Esc

Printer-friendly Version

Interactive Discussion

Table 1. Airborne data sources used in this study.

Source	Time Period	Reference	Line kilometres used
CReSIS	1993–2009	(Gogineni et al., 2001)	154 400
Operation IceBridge	2010–2011	(Studinger et al., 2010)	106 600
Alfred-Wegener-Institut	1996–1999, 2004, 2010	(Nixdorf et al., 1999)	58 350
Warm Ice Sounding Explorer	2008–2010		13 180
Pathfinder Advanced Radar Ice Sounder	2009	(Raney, 2010)	5880
High-Capability Radar Sounder	2011	(Peters et al., 2007, 2005)	5270
Technical University of Denmark	1970's	(Bamber et al., 2001b)	485*

* Approximately 30 000 km of line km were flown by TUD but we only used these data if no other, more recent, observations were available. Hence the lower number shown in Table 1.

Table 2. Inter-track differences for intra-instrument campaigns: i.e. the differences are estimated for CreSIS vs. CreSIS, AWI vs. AWI etc. only.

Data Source	Standard deviation	Number of differences
CReSIS 90's	47.95	52621
CReSIS 00's	58.27	15 240 399
AWI	11.18	154
WISE	90.87	22
HICARS	54.56	8 033 817
PARIS	20.27	3327
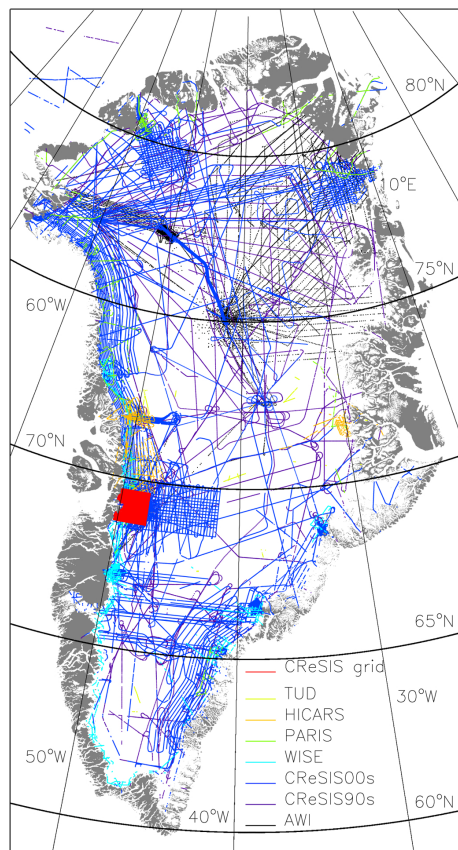
Fig. 1. Data sources. CReSIS90 includes all data from 1993 to 1999 as used in Bamber et al. (2001b). CReSIS00 includes all data derived from CReSIS instruments between 2000 and 2010 including Operation IceBridge data.

Full Screen / Esc

Printer-friendly Version

Interactive Discussion
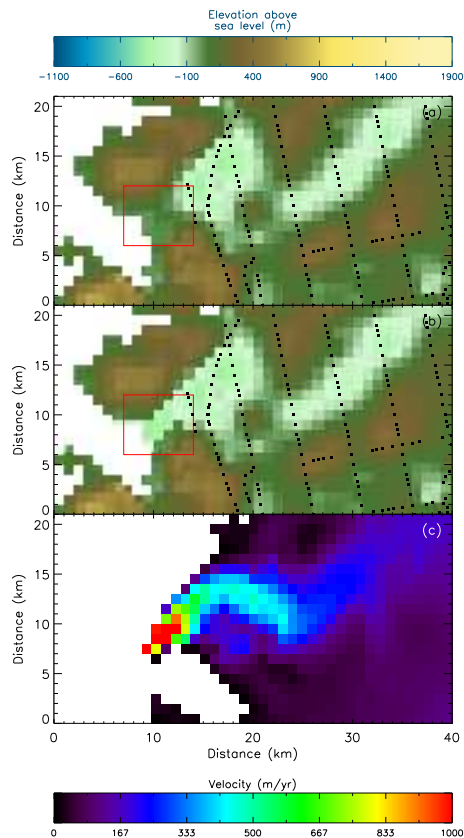
Fig. 2. (a) Outlet glacier on the north-west coast before mass conservation approach was applied. Red box outlines the area where the mass conservation approach altered the bed elevations. The location of the region is shown in the blue rectangle on Fig. 3. **(b)** Bed elevation after mass conservation has been applied in the topographically constrained fast flow region. **(c)** Ice surface velocity resampled to 1 km postings (Joughin et al., 2010).
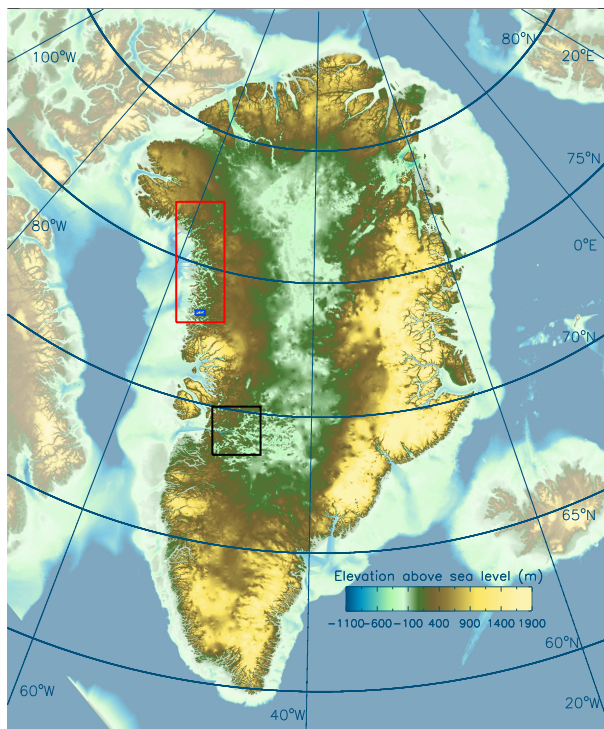
Fig. 3. Bed elevation and bathymetry in m relative to the EIGEN-GL04C geoid. Bathymetry is plotted on an opaque scale. Black and red boxes show the location of the Jakobshavn and north-west coastal regions shown in Figs. 4a–c and d–f, respectively. The blue box shows the location of the region shown in Fig. 2.
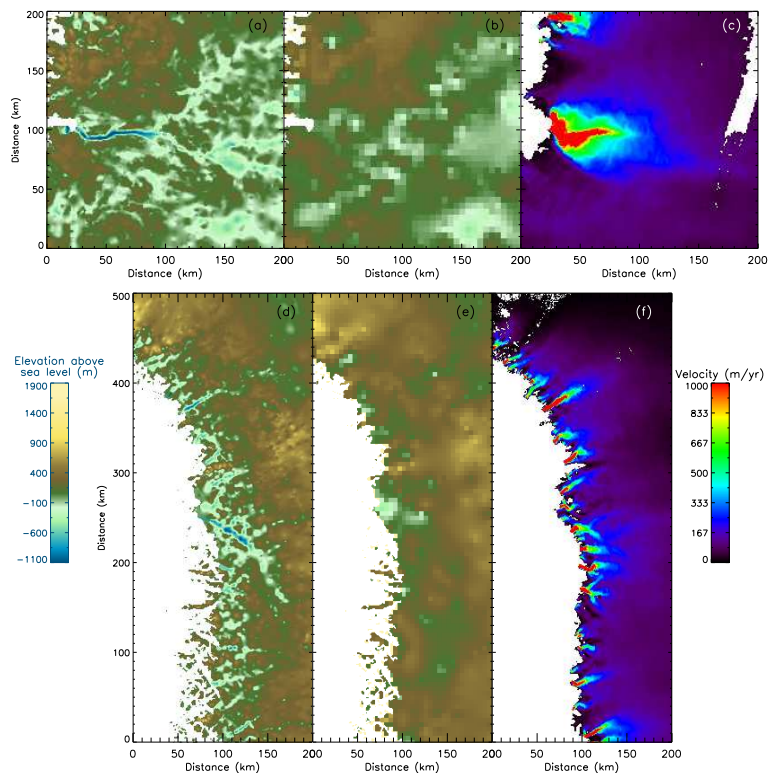
Fig. 4. **(a)** Bed elevation for Jakobshavn sector from the new DEM, **(b)** as for **(a)** but from old DEM (Bamber et al., 2001b), **(c)** ice surface velocity from InSAR (Joughin et al., 2010), **(d)** bed elevation along north-west coast from the new DEM, **(e)** as for **(d)** but from old DEM (Bamber et al., 2001b) and **(f)** ice surface velocity from InSAR (Joughin et al., 2010). For locations of the regions shown, see Fig. 3.

Full Screen / Esc
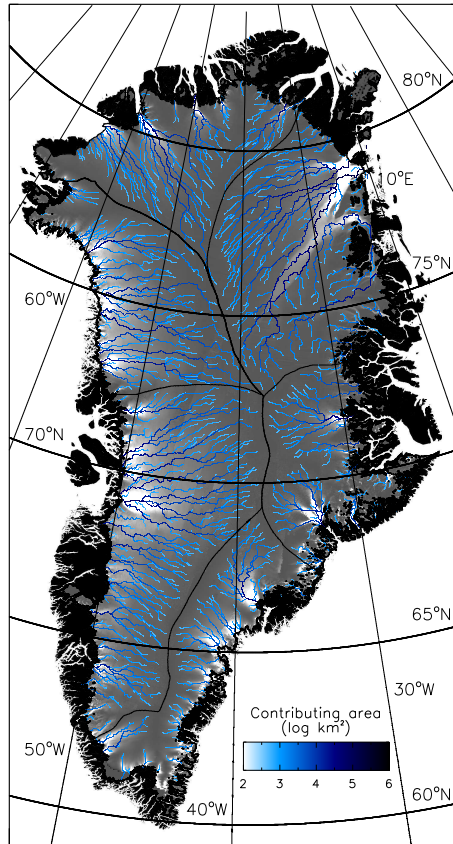
Fig. 5. Potential subglacial water flow routes. Colour scale for the flow paths indicates the potential volume of water for a uniform basal melt rate. The grey scale background shows the ice surface velocity scaled between 0 and $200\,\mathrm{m\,a^{-1}}$.
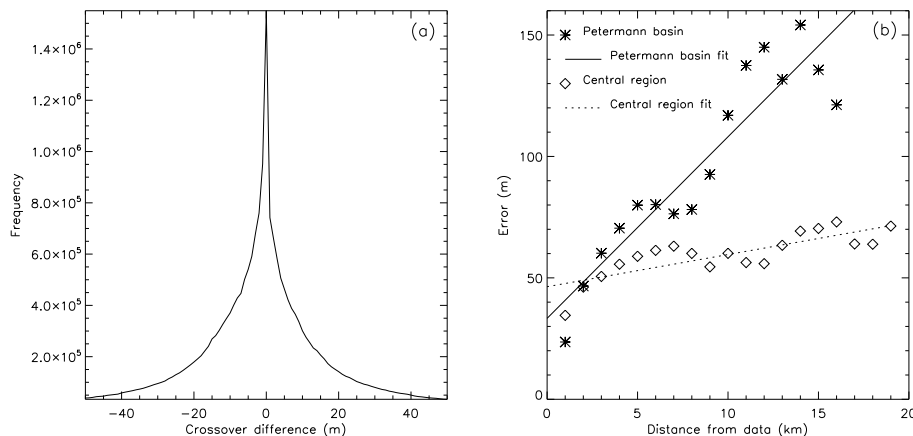
Fig. 6. (a) Histogram of inter-track, intra-instrument differences for all airborne datapoints within 50 m of each other. **(b)** Standard deviation of difference between bed elevations created using all data and using a sub-set of the data in the Petermann basin (asterisks) and the central region (diamonds). A linear least squares fit to the data is shown as solid (Petermann) and dashed (central) lines.
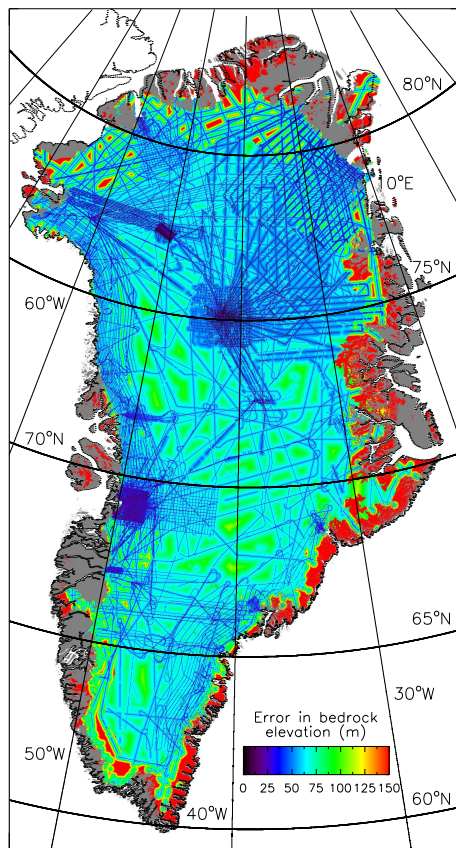
Fig. 7. RMS error in bed elevation due to uncertainties in the IPR data and the interpolation.

Printer-friendly Version

Interactive Discussion